Human Movement Science 49 (2016) 104–115

Contents lists available at ScienceDirect

Human Movement Science

journal homepage: www.elsevier.com/locate/humov

Full Length Article

Comprehensive quantitative investigation of arm swing during walking at various speed and surface slope conditions

Babak Hejrati [a,*], Sam Chesebrough [a], K. Bo Foreman [b], Jake J. Abbott [a], Andrew S. Merryweather [a]

[a] Department of Mechanical Engineering, University of Utah, United States
[b] Department of Physical Therapy, University of Utah, United States

ARTICLE INFO

Article history:
Received 27 October 2015
Revised 5 June 2016
Accepted 5 June 2016

Keywords:
Shoulder joint angle
Elbow joint angle
Motion capture
Gait rehabilitation
Gait training

ABSTRACT

Previous studies have shown that inclusion of arm swing in gait rehabilitation leads to more effective walking recovery in patients with walking impairments. However, little is known about the correct arm-swing trajectories to be used in gait rehabilitation given the fact that changes in walking conditions affect arm-swing patterns. In this paper we present a comprehensive look at the effects of a variety of conditions on arm-swing patterns during walking. The results describe the effects of surface slope, walking speed, and physical characteristics on arm-swing patterns in healthy individuals. We propose data-driven mathematical models to describe arm-swing trajectories. Thirty individuals (fifteen females and fifteen males) with a wide range of height (1.58–1.91 m) and body mass (49–98 kg), participated in our study. Based on their self-selected walking speed, each participant performed walking trials with four speeds on five surface slopes while their whole-body kinematics were recorded. Statistical analysis showed that walking speed, surface slope, and height were the major factors influencing arm swing during locomotion. The results demonstrate that data-driven models can successfully describe arm-swing trajectories for normal gait under varying walking conditions. The findings also provide insight into the behavior of the elbow during walking.

1. Introduction

Arm swing, which is characterized primarily by arm flexion/extension in the sagittal plane, contributes to balance (Behrman et al., 2000; Brujin, Meijer, Beek, & van Dieen, 2010), regulates rotational body motion Elftman, 1939, and increases metabolic efficiency Collins, Adamczyk, and Kuo, 2009 during locomotion of humans. Most clinical and modeling studies on gait tend to ignore arm swing altogether Pieter, Brujin, and Duysens, 2013. Gait rehabilitation is often focused on the legs and neglect the role of the upper limbs. However, studies show that there are neural couplings between the upper and lower limbs (Behrman et al., 2000) that can be exploited and may improve gait training (Ferris, Huang, & Kao, 2006; Marigold & Misiaszek, 2009; de Kamd, Duysens, & Dietz, 2013). New findings also capitalize on the significant role of exaggerated arm swing in improving dynamic stability during walking, which can be utilized for gait training of patients with walking impairments (Wu et al., 2016; Punt, Bruijn, Wittink, & van Dieën, 2015; Nakakubo et al., 2014). The effect of arm-swing integration in gait rehabilitation becomes more pronounced when patients practice correct arm-swing patterns (de Kamd et al., 2013). However, such patients may have impaired or abnormal arm-swing patterns (Pieter et al., 2013;

* Corresponding author.
E-mail address: babak.hejrati@utah.edu (B. Hejrati).

http://dx.doi.org/10.1016/j.humov.2016.06.001
0167-9457/

Stephenson, Lamontagne, & De Serres, 2009; Tester et al., 2011; Ford, Wagenaar, & Newell, 2007; Wagenaar & van Emmerik, 1994; Tester, Barbeau, Howand, Cantrell, & Behrman, 2012; Meyns et al., 2012; Ford, Wagenaar, & Newell, 2007), and may require assistance to attain a more natural arm-swing pattern. Thus, the integration of arm swing in gait rehabilitation may lead to more effective walking recovery for patients with walking impairments (Ferris et al., 2006; de Kamd et al., 2013; Stephenson et al., 2009; Sylos-Labini et al., 2014). Robotic or other devices for gait rehabilitation should take this integration into account in their design (Ferris et al., 2006; de Kamd et al., 2013).

Although the integration of arm swing in gait rehabilitation has been attempted by previous studies (Ferris et al., 2006; Yoon, Novandy, Yoon, & Park, 2010; Barnes, Hejrati, & Abbott, 2015), a fundamental question still needs to be answered: What are the correct and normal arm-swing trajectories that should be utilized for gait rehabilitation and assessment under various conditions? Most studies that propose models for describing arm swing during walking have been motivated to answer the question of whether arm swing is passive or active. Elftman (Elftman, 1939) and others (Collins et al., 2009, Pontzer, Holloway, Raichlen, & Lieberman, 2009, 1990, 2012) have reported shoulder moment peaks using inverse dynamics and motion capture. Since shoulder moments vary significantly in these studies, mechanisms other than the acceleration of the shoulder and gravity likely contribute to arm swing (Pieter et al., 2013). Goudriaan et al. (Goudriaan, Jonkers, van Dieen, & Bruijn, 2014) used a musculoskeletal model in OpenSim and found that muscle activity is needed to obtain correct arm swing amplitude and relative phase. Arms have also been modeled as double pendulums in which the muscle activities have been excluded from the model. Jackson, Joseph, and Wyard (1978) utilized the double pendulum model for the first time to explain arm swing, however, their model lacked proper estimation of several key parameters. The interlimb coordination and transition from 2:1 to 1:1 in arm-to-leg swing frequency ratio were investigated, where a driven pendulum model was used to explain arm movements (Kubo, Wagenaar, Saltzman, & Holt, 2004; Webb, Tuttle, & Baksh, 1994; Wagenaar & van Emmerik, 2000; Carpinella, Paolo, & Rabuffetti, 2010). Also, a multibody model was developed for simulation of human locomotion by capitalizing on the relationship between arm swing and foot reaction moments (Park, 2008). Although arm swing can be partially explained by passive dynamics, the finding of EMG activities in arm muscles suggests that passive models alone cannot adequately represent arm swing during normal walking (Kuhtz-Buschbeck & Jing, 2012; Barthelemy & Nielsen, 2010). Since further investigation is still required to determine the extent to which arm swing is passive, most current models may not rely on valid assumptions for describing arm swing during locomotion.

As mentioned earlier, current models try to provide an insight into the mechanism of arm swing, but they may not be appropriate to generate normal arm-swing trajectories for integrating arm swing into gait rehabilitation. Most models have been derived using small samples of human subjects performing a limited number of experimental conditions, and they require the measurement of the arms' and joints' mechanical properties, which are not straightforward to obtain. In addition, gait rehabilitation that includes walking on different surface slopes has been recommended as a preferred training strategy for improving balance and walking ability to prepare patients for functioning in the community (Park & Hwangbo, 2015; Desrosiers, Nadeau, & Duclos, 2015). Arm swing should be considered in slope-walking gait rehabilitation due to its important role in balance and walking ability. Although the effect of surface slope on lower-limb movements has been reported in many studies (Kawamura, Tokuhiro, & Takechi, 1991; Prentice, Hasler, Groves, & Frank, 2004; Dixon & Pearsall, 2010; Tulchin, Orendurff, & Karol, 2010; Major, Twiste, Kenney, & Howard, 2014), to the best of our knowledge, the effect of surface slope on arm swing has not been investigated. Therefore, previous models may not capture the variations in arm swing caused by walking in various conditions (i.e., walking at different speeds on different surface slopes).

The purpose of this study is to provide tools for enabling the integration of arm swing in gait rehabilitation by quantifying normal arm-swing trajectories. This study quantitatively investigates the effect of variations in both walking condition and an individual's physical characteristics on arm-swing patterns during walking. We propose data-driven mathematical models to describe arm-swing trajectory parameters given the mentioned variations. To the best of our knowledge, this is the first time that the effect of surface slope, along with walking speed, on arm swing is reported. We account for the variations between individuals by studying individuals with a wide range of height and body mass who represent a relatively large sample of healthy people with an equal number of male and female participants. Furthermore, this is the first time that the elbow joint angle during various walking conditions is investigated. These findings may help to provide a deeper insight into the mechanism that controls the forearm motion during human locomotion.

The data-driven models can be used to generate arm-swing trajectories in rehabilitative devices aiming to integrate arm swing in gait rehabilitation of patients with walking disabilities (Stephenson et al., 2009; Yoon et al., 2010; Barnes et al., 2015). Furthermore, the elbow joint range of motion and its relative phase with respect to the ipsilateral shoulder joint angle during walking may be useful in the design and control of powered-elbow prostheses (Fougner, Stavdahl, Kyberd, Losier, & Parker, 2012; Bennett, Mitchell, & Goldfarb, 2015).

2. Methods

2.1. Subjects

Thirty healthy subjects participated from a large sample of young individuals with healthy gait. This study was approved by the Institutional Review Board of the University of Utah. We used fifteen male and fifteen female subjects to account for the effect of gender on arm-swing patterns. The age range of our male subjects was 20–35 years (26.00 ± 4.85 years)

reported as (mean ± standard deviation), and the age range of our female subjects was 18–37 years (24.13 ± 5.16 years). Male subjects' body mass ranged from 64 to 98 kg (77.98 ± 11.59 kg), and female subjects' body mass ranged from 49 to 71 kg (61.23 ± 7.51 kg). The male subjects' height ranged from 1.70 to 1.91 m (1.80 ± 0.06 m), and the height range of female subjects was from 1.58 to 1.76 m (1.67 ± 0.04 m).

2.2. Experimental protocol

Subjects were required to find their self-selected "normal" and "fastest" walking speeds. Based on each subject's "normal" and "fastest" walking speeds, we used linear interpolation and calculated the midpoint between "normal" and "fastest" speeds to represent the "fast" speed; to calculate "slow" speed, we used linear extrapolation, such that "normal" speed is the midpoint between "slow" and "fast" speeds. Each subject tried four walking speeds as "slow", "normal", "fast", and "fastest". To investigate the effect of walking surface slope on arm swing, we utilized five slope levels in our experiments: -8.5°, -4.2°, 0°, $+4.2^{\circ}$, $+8.5^{\circ}$, respectively, where negative grades indicate decline walking and positive grades indicate incline walking. Fig. 1 shows experimental trials with various surface-slope conditions. Overall, each subject tried twenty experimental trials as the combination of four walking speeds on five surface slopes in a randomized order.

2.3. Experimental setup and data collection

During a given trial, whole-body kinematic data were recorded for 1 min by means of a ten-camera motion analysis system (NaturalPoint, Corvallis, OR) operating at 120 Hz sampling frequency. We used thorax, arm, and forearm segments based on a modified clinical model proposed by others (Petuskey, Bagley, Abdala, James, & Rab, 2007; Rab, Petuskey, & Bagley, 2002). Thorax, arm, and forearm segments and their coordinate systems were defined using markers on the sternum, C7 and T10 spinous processes, clavicle, left/right acromions, left/right medial and lateral epicondyles, and left/right distal radius and ulna landmarks. For tracking the segments during walking, marker clusters were attached to the arms and forearms.

2.4. Data processing

Marker trajectories were labeled and data were imported into Visual3D (C-Motion, Germantown, MD) where raw kinematic data were low-pass filtered (4th-order zero-lag Butterworth with cut-off frequency of 6 Hz using residual analysis (Winter, 2005)). Right-hand rule was followed to form the coordinate systems such that X directed laterally to the right, Y directed forward (anteriorly), and Z axis directed upward (superiorly). Joint angles were calculated in Visual3D using Cardan sequence $XY'Z''$ in which joint angles in the sagittal plane (flexion/extension) were around the X-axes of the proximal segments' coordinate systems.

2.5. Shoulder-angle and elbow-angle modeling

Shoulder joint angles θ_{sh} in the sagittal plane during subjects' steady-state walking were considered for representing gait-related arm swing. The shoulder-angle trajectories were segmented by the contralateral foot's heel-strikes as illustrated in Fig. 2a. A 1:1 arm-to-leg frequency coordination (i.e., one shoulder oscillation per gait cycle) in human walking is a stronger attractor pattern (Ford et al., 2007), and only 6% of our data, corresponding to very slow walking, followed a 2:1 arm-to-leg frequency pattern. Due to the importance of a 1:1 frequency pattern for gait rehabilitation (Behrman et al., 2000; Ferris et al., 2006; de Kamd et al., 2013; Ford et al., 2007), we only considered cases with a 1:1 arm-to-leg frequency ratio. At least five shoulder-angle cycles from each left and right shoulder-angle trajectories were chosen. The chosen shoulder-angle cycles were normalized to 100% of their corresponding gait cycles to superimpose the cycles within an experimental trial. The mean trajectory of the superimposed cycles were calculated to represent the mean arm-swing trajectory of a trial.

(a) (b) (c)

Fig. 1. A subject is performing the experimental trials during (a) decline walking, (b) level walking, and (c) incline walking.

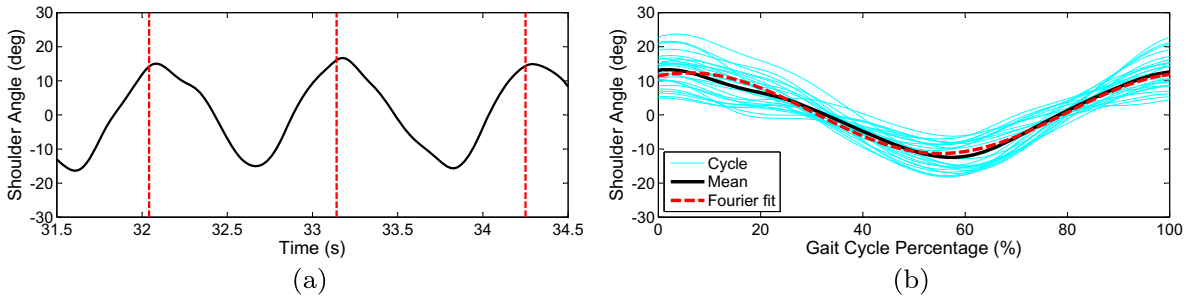

Fig. 2. (a) Right shoulder angle (solid black line) of a typical subject segmented by the left foot's heel-strikes (dashed red lines) during an experimental trial, (b) shoulder-angle cycles and the mean cycle with its Fourier fit of a typical subject within a trial. (For interpretation of the references to color in this figure legend, the reader is referred to the web version of this article.)

We approximated the mean trajectory of a trial by a sinusoid using the first harmonic (i.e., the fundamental frequency) of the Fourier series as shown in Fig. 2b. The Fourier fit of the mean shoulder-angle trajectory is given by:

$$\theta_{sh} = A_{sh}\cos(2\pi f_{sh}t + \phi_{sh}) + \theta_{0sh} \tag{1}$$

where A_{sh} is the amplitude in degrees, f_{sh} is the frequency in Hz, ϕ_{sh} is the relative Fourier phase between the shoulder angle and the contralateral foot's heel-strikes in radians, and θ_{0sh} is the offset value of the shoulder angle, which is the value that the shoulder-angle trajectory oscillates about, in degrees. To provide a better insight into the relative Fourier phase, ϕ_{sh} is presented in degrees throughout this paper, but must be converted to radians for use in Eq. (1). A positive value of θ_{sh} corresponds to shoulder flexion, and a negative value of θ_{sh} corresponds to shoulder extension, relative to θ_{0sh}.

Elbow joint angles θ_{el} in the sagittal plane were also investigated in this study. The elbow angle trajectories were segmented by the ipsilateral shoulder-angle trajectories' local maxima as illustrated in Fig. 3a. The mean trajectory of all the elbow-angle cycles were calculated as shown in Fig. 3b similar to what was done for the mean shoulder-angle trajectory.

The mean elbow-angle trajectory could not be sufficiently approximated by the first harmonic of the Fourier series. Therefore, to determine the amplitude A_{el} and offset value θ_{0el} of the mean elbow-angle trajectory, we used the trajectory's local maximum and minimum as follows:

$$A_{el} = \frac{\theta_{el,max} - \theta_{el,min}}{2} \quad \& \quad \theta_{0el} = \frac{\theta_{el,max} + \theta_{el,min}}{2} \tag{2}$$

where $\theta_{el,max}$ and $\theta_{el,min}$ indicate the maximum and minimum, respectively, of the mean elbow-joint angle in an experimental trial. Also, we calculated the point relative phase (PRP), in degrees, for gait cycle j (Stephenson et al., 2009):

$$PRP_{el/sh}(j) = \frac{t_{max\theta_{el}}(j) - t_{max\theta_{sh}}(j)}{t_{cycle}(j)} \times 360^{\circ} \tag{3}$$

where the gait cycle j was determined by two consecutive shoulder joint angle's local maxima (i.e., maximum flexion angles) as shown in Fig. 3a, $t_{cycle}(j)$ represents the time duration of gait cycle j in seconds, $t_{max\theta_{el}}(j)$ is the time at which the elbow's maximum flexion in cycle j occurs (the first maximum of the elbow angle in cycle j), and $t_{max\theta_{sh}}(j)$ is the time at which the ipsilateral shoulder's maximum flexion in cycle j occurs. A positive value of $PRP_{el/sh}$ indicates that maximum flexion of the elbow occurred after the maximum flexion of the ipsilateral shoulder, whereas a negative value indicates the opposite sequence.

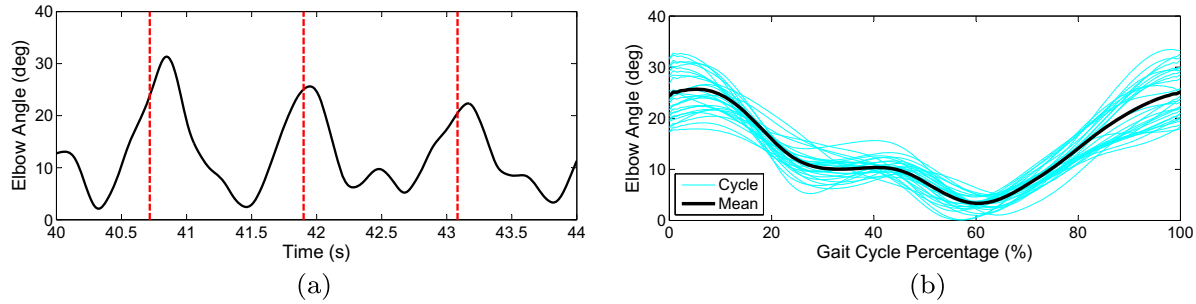

Fig. 3. (a) Right elbow joint angle of a typical subject (solid black line) segmented by the right shoulder angle's local maxima (dashed red lines), (b) elbow-angle cycles and the mean cycle of a typical subject within a trial. (For interpretation of the references to color in this figure legend, the reader is referred to the web version of this article.)

2.6. Statistical analysis

The independent variables in our statistical analysis included: height h in meters, mass m in kilograms, gender g with $g = 0$ for females and $g = 1$ for males, walking speed v in meters per second, and surface slope s in degrees. The dependent variables were the mean shoulder-angle trajectory parameters (i.e., $f_{sh},\ A_{sh},\ \theta_{0sh},\ \phi_{sh}$) and elbow-angle trajectory parameters (i.e., $A_{el},\ \theta_{0el},\ PRP_{el/sh}$). We carried out hierarchical multiple regression to investigate the contribution of each individual independent variable to the prediction of dependent variables and excluded outliers. The independent variables with larger R^2-change, F-change, and standardized coefficient have larger effect sizes than other variables. The sign of standardized coefficient shows whether an increase in the independent variable causes the dependent variable to increase (positive) or to decrease (negative). To create data-driven models for shoulder-angle and elbow-angle parameters and to avoid including unimportant terms in the model, only the significant independent variables and two-way interactions with R^2-change greater than 1% were considered.

3. Results

3.1. Model generation

Table 1 shows the significant independent variables that affect f_{sh} (with $\alpha = 0.05$). Although subjects' mass m and gender g are statistically significant, the effect sizes are substantially smaller than other variables. The shoulder-angle frequency f_{sh} increased by walking speed v, whereas it decreased by an increase in subjects' height h and surface slope s. All the variance inflationary factors (VIF) in Table 1 are less than 5 indicating that there was no multicollinearity among the significant independent variables (Snee, 1973; O'Brien, 2007). The model containing an intercept, main effects, and a two-way interaction is expressed by:

$$f_{sh}(h, v, s) = 0.361v - 0.0141s - 0.561h + 0.00340vs + 1.46 \tag{4}$$

where R^2-change due to the inclusion of most of the independent variables is already given in Table 1, and additional R^2-change by including the interaction term vs is 1.90%.

The significant independent variables that affect the amplitude of the mean shoulder-angle A_{sh} are shown in Table 2. The amplitude of the mean shoulder-angle trajectory decreased with an increase in h, whereas it increased by an increase in $v,\ m$, and s. In Eq. (5), a quadratic polynomial fits the relationship between A_{sh} and h better than a linear fit, whereas linear fits were best-fitting functions between A_{sh} and the rest of the variables.

$$A_{sh}(h, m, v, s) = -359h + 74.07v + 107h^2 + 0.289mv - 0.267m - 50.1hv + 0.0995s + 323 \tag{5}$$

where R^2-changes due to the use of the quadratic term h^2, and the interaction terms mv and hv are 2.40%, 2.10%, and 1.15%, respectively. R^2-changes due to the use of the other independent variables is already given in Table 2.

The offset value of the mean shoulder-angle trajectory θ_{0sh} was most significantly influenced by the walking surface slope s as shown in Table 3. Subjects leaned forward during incline walking, thus their arm swing occurred in more flexed angle (i.e., $\theta_{0sh} > 0$), whereas subjects leaned backward during decline walking and arm swing occurred in more extended angle ($\theta_{0sh} < 0$).

Linear fits were used to represent the relationships between θ_{0sh} and the variables in Eq. (6) since other higher-order polynomials did not improve the fits.

$$\theta_0(h, v, s) = 0.160s - 12.3h - 2.28v + 0.246vs + 25.2 \tag{6}$$

where R^2-change due to the inclusion of most of the independent variables is already given in Table 3, and additional R^2-change by including the interaction term vs is 2.00%.

The relative Fourier phase of the mean shoulder-angle trajectory ϕ_{sh} is the phase between the shoulder angle and the contralateral foot's heel-strikes. When $\phi_{sh} > 0^\circ$, it indicates that maximum flexion of the shoulder angle precedes the contralateral foot's heel-strike in a cycle, whereas $\phi_{sh} < 0^\circ$ indicates the opposite sequence. Table 4 shows the significant independent variables.

Table 1
Statistical analysis for f_{sh} where variables are organized by decreasing R^2-change.

Independent variable	R^2 change (%)	F change	Standardized coefficients	Collinearity VIF
Speed (v)	56.8	703.92	0.76	1.02
Slope (s)	10.8	211.00	−0.34	1.00
Height (h)	2.7	23.69	−0.24	2.94
Mass (m)	0.2	1.06	−0.13	2.32
Gender (g)	0.02	0.12	0.10	2.38

Table 2
Statistical analysis for A_{sh} where variables are organized by decreasing R^2-change.

Independent variable	R^2 change (%)	F change	Standardized coefficients	Collinearity VIF
Height (h)	22.00	142.10	−0.63	2.94
Speed (v)	20.05	185.33	0.45	1.02
Mass (m)	2.00	13.50	0.19	2.32
Slope (s)	1.10	10.31	0.10	1.00

Table 3
Statistical analysis for θ_{0sh} where variables are organized by decreasing R^2-change.

Independent variable	R^2 change (%)	F change	Standardized coefficients	Collinearity VIF
Slope (s)	36.70	325.11	0.60	1.00
Height (h)	4.50	28.49	−0.30	2.94
Speed (v)	2.80	14.82	−0.19	1.02
Mass (m)	0.60	2.99	0.10	2.32

At slower walking speeds the maximum shoulder flexion preceded the contralateral foot's heel-strikes ($\phi_{sh} > 0^\circ$), and as walking speed increased the mentioned pattern became reversed ($\phi_{sh} < 0^\circ$); the opposite trend exists for the relationship between ϕ_{sh} and s such that as the slope increased from decline walking ($s < 0^\circ$) to incline walking ($s > 0^\circ$), the value of ϕ_{sh} changed from negative to positive. Gender g had a small effect size compared to the effect size of speed v and slope s. The proposed model expressed in Eq. (7) utilizes linear fits for explaining the relationships between ϕ_{sh} and the significant independent variables.

$$\phi_{sh}(g, v, s) = -40.2v + 1.55s + 8.26g + 41.2 \tag{7}$$

Table 5 shows the significant independent variables influencing A_{el} and their effect sizes. The amplitude A_{el} increases significantly as walking speed v increases, and A_{el} decreases as the surface slope s changes from decline to incline condition; female subjects has slightly larger A_{el} than male subjects. Linear fits were used in Eq. (8) to describe the relationships between A_{el} and the variables.

$$A_{el}(g, v, s) = 6.39v - 1.59g + 0.117s - 0.182vs + 0.101 \tag{8}$$

where R^2-change due to the inclusion of most of the independent variables is already given in Table 5, and additional R^2-change by including the interaction term vs is 1.78%.

Table 6 shows the significant independent variables influencing θ_{0el} and their effect sizes, which are similar to what was described for A_{el}. The offset values of the mean elbow angles, unlike the offset values of the mean shoulder angles, were always greater than zero, since the elbow joint angles were always flexed during locomotion. Linear fits were used to describe the relationships between θ_{0el} and the variables in Eq. (9).

$$\theta_{0el}(g, v, s) = 26.4v - 6.69g + 0.458s - 0.722vs + 2.155 \tag{9}$$

where R^2-change due to the inclusion of most of the independent variables is already given in Table 6, and additional R^2-change by including the interaction term vs is 1.13%.

The point relative phase between the ipsilateral shoulder and elbow joint angles, $PRP_{el/sh}$, provides insight into the coordination of the shoulder and elbow angles during walking. The results of statistical analysis in Table 7 show that height h, speed v, and mass m were significant independent variables influencing $PRP_{el/sh}$, however, they had small effect sizes.

3.2. Model analysis

To evaluate the proposed models in Section 3.1 for calculating the shoulder-angle and elbow-angle parameters, we analyzed the relationship and residual errors between the shoulder-angle and elbow-angle parameters predicted by the models denoted by $(f_{sh,p}, A_{sh,p}, \theta_{0sh,p}, \phi_{sh,p}, A_{el,p}, \theta_{0el,p})$ and the same parameters obtained from kinematic measurements $(f_{sh,m}, A_{sh,m}, \theta_{0sh,m}, \phi_{sh,m}, A_{el,m}, \theta_{0el,m})$.

Table 4
Statistical analysis for ϕ_{sh} where variables are organized by decreasing R^2-change.

Independent variable	R^2 change (%)	F change	Standardized coefficients	Collinearity VIF
Speed (v)	38.00	299.05	−0.62	1.02
Slope(s)	15.60	167.00	0.39	1.00
Gender(g)	1.80	8.67	0.12	2.38

Table 5
Statistical analysis for A_{el} where variables are organized by decreasing R^2-change.

Independent variable	R^2 change (%)	F change	Standardized coefficients	Collinearity statistics	
				Tolerance	VIF
Speed (v)	40.40	384.53	0.64	0.98	1.02
Gender (g)	5.90	31.72	−0.28	0.42	2.38
Slope (s)	2.50	24.87	−0.15	1.00	1.00

Table 6
Statistical analysis for θ_{0el} where variables are organized by decreasing R^2-change.

Independent variable	R^2 change (%)	F change	Standardized coefficients	Collinearity statistics	
				Tolerance	VIF
Speed (v)	40.50	389.78	0.64	0.98	1.02
Gender (g)	6.20	33.74	−0.29	0.42	2.38
Slope (s)	2.40	24.08	−0.15	1.00	1.00

Table 7
Statistical analysis for $PRP_{el/sh}$ where variables are organized by decreasing R^2-change.

Independent variable	R^2 change (%)	F change	Standardized coefficients	Collinearity statistics	
				Tolerance	VIF
Height (h)	13.30	83.49	−0.21	0.34	2.94
Speed (v)	3.70	24.26	0.19	0.98	1.02
Mass (m)	1.10	6.83	−0.16	0.43	2.32

Fig. 4 depicts the measured parameters versus the predicted ones, where each data point in the plots represents a pair of predicted and measured values, e.g. ($f_{sh,p}$, $f_{sh,m}$). The thick line in each plot expressed by $y_m = ax_p + b$ indicates the best-fit line between predicted and measured values, where (x_p, y_m) could take any of the mentioned paired values, and a and b are the line's slope and intercept, respectively (ideally, $a = 1$ and $b = 0$). The thin lines in each plot, parallel with the thick lines, illustrate 95% prediction bands for the best-fit lines. The prediction band sizes for f_{sh}, A_{sh}, θ_{0sh}, ϕ_{sh}, A_{el}, and θ_{0el} are (±0.18 Hz), (±7.8°), (±6.3°), (±31°), (±5.3°), and (±22°) respectively. The prediction bands in each plot cover an area into which we expect future data points in the form of (predicted,measured) to fall.

Table 8 shows the goodness of the fit in terms of R^2 and root-mean-squared error (RMSE) of the proposed models in Section 3.1; it also represents the mean value and 95% confidence interval of each best-fit line's slope and intercept (Fig. 4), and the mean value and (min,max) of the residuals. The coefficient of determinations R^2 in Table 8 indicate that the models sufficiently explain the variations in the shoulder-angle parameters. The slope a and intercept b of the best-fit lines for each plot are almost equal to one and zero, respectively, implying that the six models adequately describe the kinematic measurements. The mean value of residuals for each model was zero and the minimum and maximum errors across the range of predictions were almost symmetric. Residual analysis suggested that the prediction errors were random, thus there was no need to improve the proposed models by including extra variables, using higher-order terms, or considering more complex interaction terms. A leave-one-out cross-validation procedure (Lenhoff et al., 1999) was used to estimate the true achieved coverage of the prediction bands. The cross-validation analysis demonstrated that the true coverage probabilities for f_{sh}, A_{sh}, θ_{0sh}, ϕ_{sh}, A_{el}, and θ_{0el} were 94%, 94%, 96%, 95%, 94%, and 94%, respectively. Since the true coverage probabilities were close to the desired value of 95%, we conclude that the prediction bands were able to capture the normal ranges of the parameters (Anderst, 2015).

We used the proposed shoulder-angle models in Section 3.1 to describe the shoulder-angle trajectories as follows:

$$\theta_{sh,p}(h, m, g, v, s) = A_{sh}\cos(2\pi f_{sh}t + \phi_{sh}) + \theta_{0sh} \tag{10}$$

Fig. 5 illustrates a few examples of the shoulder-angle trajectory described by Eq. (10) and the actual mean shoulder-angle trajectory for an individual participant and walking condition. The coefficient of determination R^2 was used as the goodness of the model in Eq. (10), where the described angles were compared with the actual angles obtained by kinematic measurements. The mean value of R^2 and RMSE between described and measured trajectories (with their 95% confidence intervals) are 69.19% (66.63%,71.75%) and 4.83° (4.61°, 5.05°), respectively. Also, the range of motion of the described shoulder trajectories with the mean value of 28.93° (28.21°, 29.66°) were similar to the range of motion of the actual shoulder angles with the mean value of 29.64° (28.60°, 30.69°) with no statistically significant difference ($p = 0.27$) between their mean values. The results indicate that the proposed models properly describe shoulder-angle trajectories for our study population across all conditions.

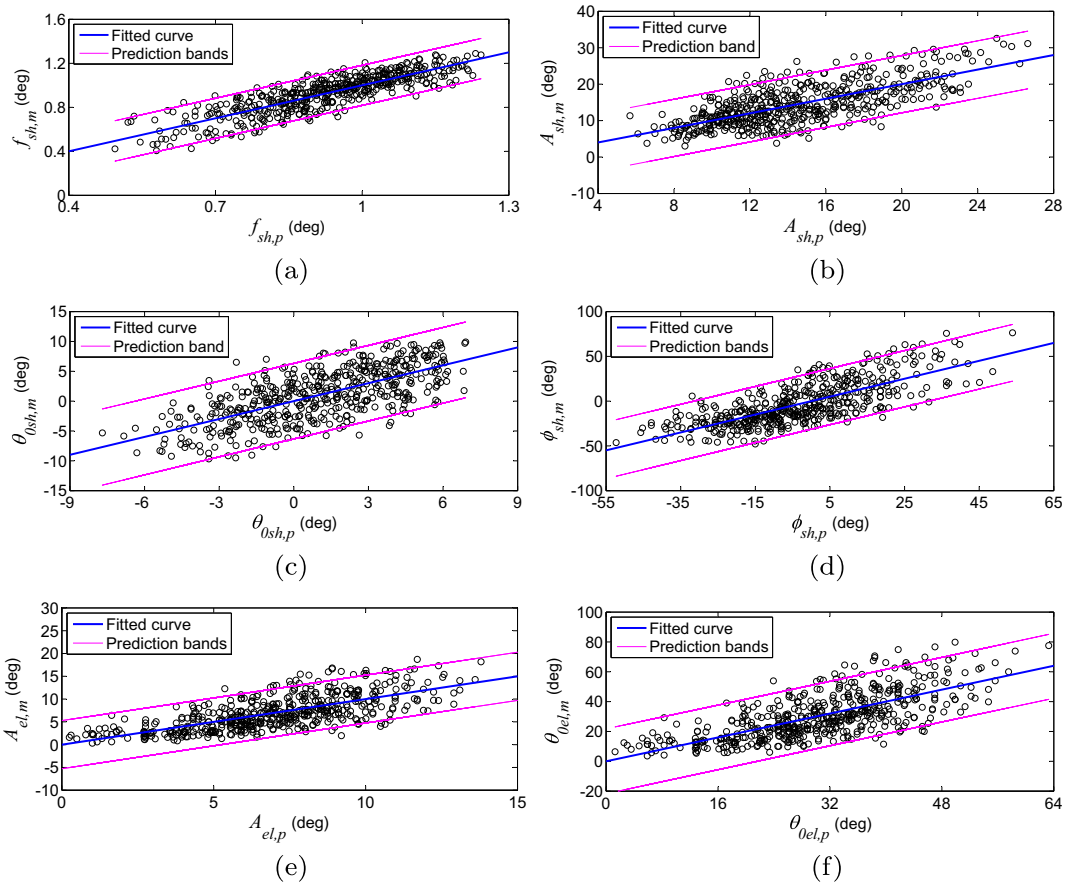

Fig. 4. Predicted and measured values for (a) f_{sh}, (b) A_{sh}, (c) θ_{0sh}, (d) ϕ_{sh}, (e) A_{el}, and (f) θ_{0el}. Data is shown for all subjects. Each data point represents an individual trial.

Table 8
Quantitative analysis of the proposed models in terms of coefficient of determination, prediction-measurement relationship, and residual analysis.

Model (variables)	R^2 (%)	RMSE (Units)	a (CI)	b (CI)	Residual mean (min,max)
$f_{sh}(h, v, s)$	72.2	0.09 (Hz)	1(0.94,1.05)	0(−0.05,0.05)	0(−0.23,0.20)
$A_{sh}(h, m, v, s)$	50.8	3.98 (deg)	1(0.91,1.08)	0(−1.26,1.26)	0(−10.6,11.7)
$\theta_{0sh}(h, v, s)$	46.0	3.20 (deg)	1(0.90,1.09)	0(−0.30,0.30)	0(−8.33,8.81)
$\phi(g, v, s)$	55.4	15.90 (deg)	1(0.92,1.07)	0(−1.46,1.46)	0(−37.35,39.45)
$\hat{A}_{el}(g, v, s)$	50.5	2.66 (deg)	1(0.91,1.08)	0(−0.64,0.64)	0(−7.24,7.92)
$\theta_{0el}(g, v, s)$	50.2	10.95 (deg)	1(0.91,1.08)	0(−2.78,2.78)	0(−28.21,33.07)

Statistical analysis of $PRP_{el/sh}$ did not indicate any significant independent variable with a considerable effect size, thus the multiple linear regression could not explain an acceptable portion of variations in $PRP_{el/sh}$ (i.e., $R^2 = 18.4\%$). The residual analysis of $PRP_{el/sh}$ shown in Fig. 6a indicated two distinct patterns. These two patterns could be differentiated by labeling the residuals located on a straight line in Fig. 6a as Pattern 1 and labeling the rest of the residuals as Pattern 2. Fig. 6b illustrates an example of the elbow joint angle during Pattern 1, in which $PRP_{el/sh}$ is very close to zero, indicating that the maximum elbow flexion occurred at approximately the same time as the maximum ipsilateral shoulder flexion. Fig. 6c shows an example of the elbow joint angle during Pattern 2, in which $PRP_{el/sh}$ is significantly greater than zero, indicating that there was a significant time lag in the occurrence of the maximum elbow flexion relative to the maximum ipsilateral shoulder flexion.

Both patterns were observed across all walking conditions and participants' physical characteristics, therefore both patterns can be considered as normal elbow movement during locomotion. However, Pattern 2, where significant lag exists, was observed more frequently (67% of trials) than Pattern 1 (33% of trials). Since a multiple linear regression model could not

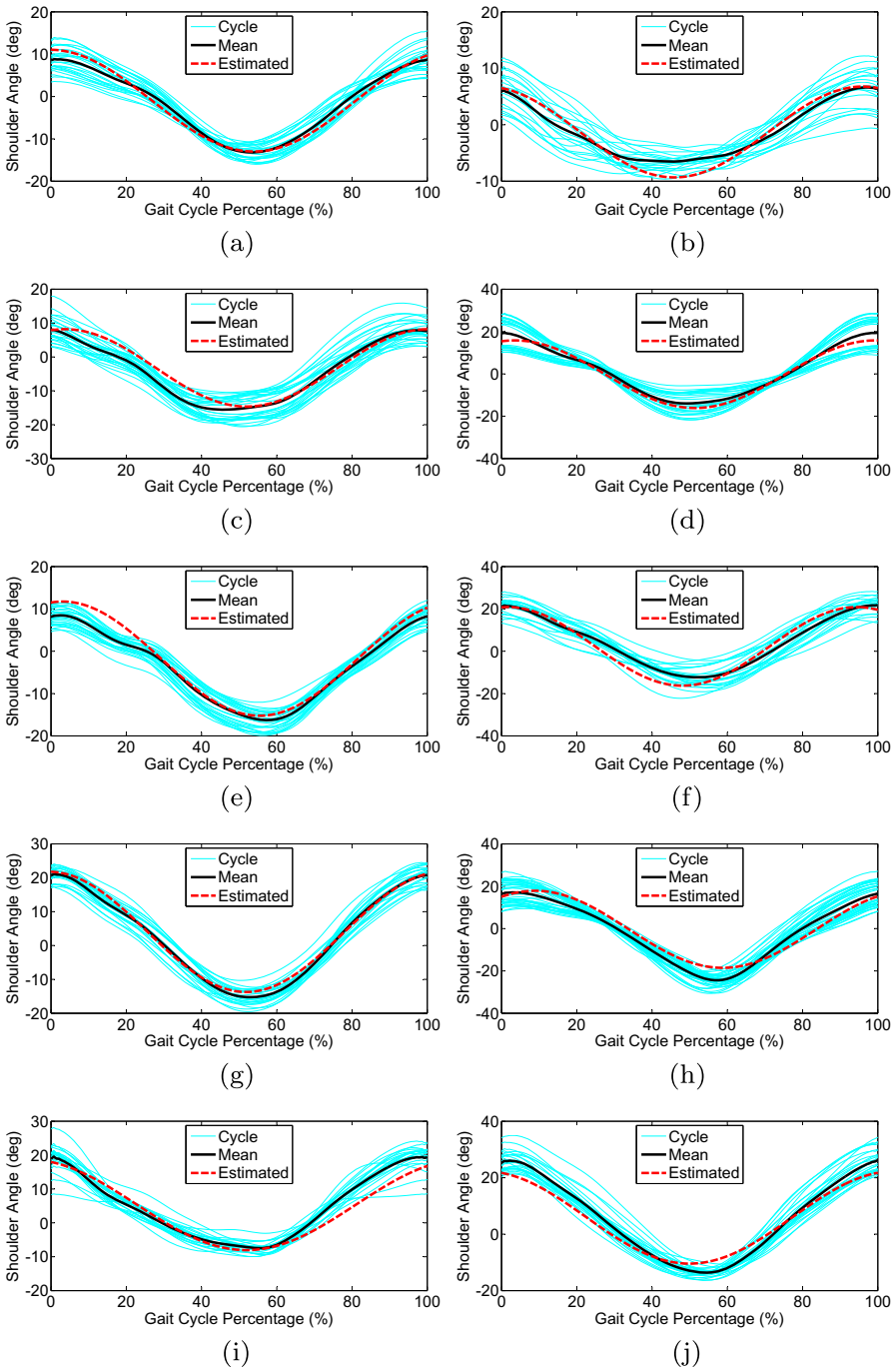

Fig. 5. Comparison between the described and measured shoulder-angle trajectories for the values of (h, m, g, v, s) as follows: (a) (1.70,74,1,0.88,−8.5), (b) (1.85,72,1,0.52,−8.5), (c) (1.87,84,1,1.40,−4.2), (d) (1.68,65,0,1.18,−4.2), (e) (1.91,98,1,1.5,0), (f) (1.64,60,0,1.2,0), (g) (1.66,67,0,1.14,4.2), (h) (1.91,97,1,2.2,4.2), (i) (1.71,71,0,0.88,8.5), and (j) (1.66,67,0,0.96,8.5).

sufficiently account for the presence of both patterns, we present $PRP_{el/sh}$ with two distributions. The mean values (± standard deviation) of Pattern 1 and Patterns 2 are 3.25°(±0.65°) and 23.66°(±8.22°), respectively.

4. Discussion

To address the limitations of existing arm-swing models, we proposed data-driven models based on statistical analyses of the upper-extremities during various walking conditions. The data-driven models simply require five independent vari-

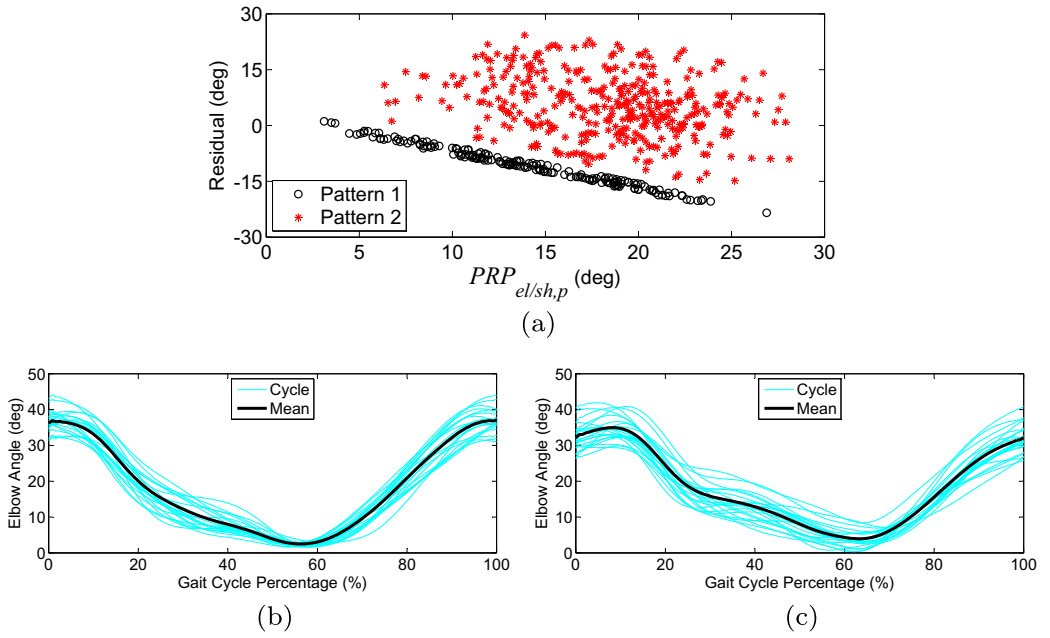

Fig. 6. (a) Residual plot of the multiple linear regression model for $PRP_{el/sh}$. The black circles demonstrate Pattern 1, with typical cycles shown in (b), where $PRP_{el/sh}$ is close to zero. The red asterisks demonstrate Pattern 2, with typical cycles shown in (c), where $PRP_{el/sh}$ is significantly greater than zero.

ables—height, mass, gender, walking speed, and surface slope—to describe the shoulder-angle parameters such as frequency, amplitude, offset value, and phase, as well as the elbow-angle amplitude and offset value. The trajectories generated by Eq. (10) may be useful for robotic (Yoon et al., 2010; Barnes et al., 2015) or other rehabilitation devices (Ferris et al., 2006; Stephenson et al., 2009) that integrate arm swing in gait rehabilitation. Eq. (10 can use a patient's physical information as primary inputs, and walking speed and surface slope can be measured during walking or be provided as predetermined values to generate desired shoulder-angle trajectories. These trajectories can be applied to the patient by means of devices similar to what is proposed in Yoon et al. (2010) and Barnes et al. (2015) to correct the patient's arm swing for more effective gait rehabilitation.

In addition, given the fact that analyzing arm-swing patterns in terms of their amplitude and coordination with lower limbs (interlimb coordination) have become increasingly important in rehabilitation of patients with different walking disabilities (Stephenson et al., 2009; Huang et al., 2011; Tester et al., 2012), the plots in Fig. 4 may serve as guidelines for diagnosis and assessment of a patients' arm swing.

We also studied the effect of various walking conditions and participants' physical characteristics on elbow-angle parameters. Although walking speed, surface slope, and gender were statistically significant variables, walking speed had a larger effect size than surface slope and gender. We observed two patterns in the point relative phase between ipsilateral shoulder and elbow angles. These results may be helpful for providing a deeper insight into the mechanism that controls the forearm motion during locomotion. However, more studies are required to consider the muscle activities of upper limbs for better understanding of this mechanism.

Our results may be particularly useful for rehabilitation of patients with spinal cord injury since the age group of our participants closely matches those experiencing spinal cord injury (Gil-Agudo et al., 2011). Furthermore, with the addition of older subjects to this study the results could be expanded to help rehabilitate older individuals who have experienced upper-extremity involvement due to injuries such as stroke and Parkinson disease.

5. Conclusion

We investigated the effect of several key factors that influence arm-swing patterns during walking. Although the effect of slope on human walking has been studied in the literature, to our knowledge, this work is the first to report the effect of slope on arm swing. Our participants performed a wide range of walking speeds (0.22–2.2 m/s) based on their own self-selected speeds during the experiments. In this study, we used a large number of participants who represented a wide range of height and mass. Equal numbers of male and female participants were used in the experiments to account for any possible effect of gender on arm swing during walking.

We found that walking speed, surface slope, and individuals' height were the most important factors influencing arm swing during walking. These factors most frequently appeared as significant independent variables with a large effect size

in statistical analyses. The shoulder-angle frequency and amplitude increased directly as walking speed increased. Participants' mass and gender were not as influential as height and their effect sizes were small in the statistical analyses.

Our results show that data-driven models can successfully describe arm-swing for normal gait under varying walking conditions. The data-driven models can be used to generate arm-swing-like trajectories for integration of arm swing in gait rehabilitation, for gait assessment of patients with walking disabilities, or for the control of powered-elbow prostheses. The findings also may provide a better insight into how the forearm moves during walking in various conditions.

Acknowledgments

The authors would like to thank Dr. John M. Hollerbach for his support and Alexandra M. Shamir for her assistance in data processing. This work was supported by the National Science Foundation through grant 1208637.

References

Anderst, W. J. (2015). Bootstrap prediction bands for cervical spine intervertebral kinematics during in vivo three-dimensional head movements. *Journal of Biomechanics, 48*, 1270–1276.
Barnes, O. R., Hejrati, B., & Abbott, J. J. (2015). An underactuated wearable arm-swing rehabilitator for gait training. In *IEEE international conference on robotics and automation* (pp. 4998–5003).
Barthelemy, D., & Nielsen, J. B. (2010). Corticospinal contribution to arm muscle activity during human walking. *Journal of Physiology, 588*, 967–979.
Behrman, A. L., & Harkema, S. J. (2000). Locomotor training after human spinal cord injury: A series of case studies. *Physical Therapy, 80*(7), 688–700.
Bennett, D. A., Mitchell, J., & Goldfarb, M. (2015). Design and characterization of a powered elbow prosthesis. In *International conference of the IEEE EMBS* (pp. 2458–2461).
Brujin, S. M., Meijer, O. G., Beek, P. J., & van Dieen, J. H. (2010). The effects of arm swing on human gait stability. *Journal of Experimental Biology, 213*, 3945–3952.
Carpinella, H., Paolo, C., & Rabuffetti, M. (2010). Coordination between upper- and lower-limb movements is different during overground and treadmill walking. *European Journal of Applied Physiology, 108*, 71–82.
Cimolin, V., Galli, M., Albertini, G., Crivellini, M., & Romkes, J. (2012). Quantitative analysis of upper limbs during gait: a marker set protocol. *Journal of Applied Biomaterials and Functional Materials, 10*(1), 49–55.
Collins, S. H., Adamczyk, P. G., & Kuo, D. (2009). Dynamic arm swing in human walking. *Proceedings of the Royal Society of London Series B, 276*, 3679–3688.
de Kamd, D., Duysens, J., & Dietz, V. (2013). Do we need allowing arm movements for rehabilitation of gait? In *Converging clinical and engineering research on neurorehabilitation* (pp. 959–962). Springer-Verlag.
Desrosiers, É., Nadeau, S., & Duclos, C. (2015). Balance during walking on an inclined instrumented pathway following incomplete spinal cord injury. *Spinal Cord, 53*, 387–394.
Dixon, P. C., & Pearsall, D. J. (2010). Gait dynamics on a cross-slope walking surface. *Journal of Applied Biomechanics, 26*(1), 17–25.
Elftman, H. (1939). The function of the arms in walking. *Human Biology, 11*(4), 529–535.
Ferris, D. P., Huang, H. J., & Kao, P. C. (2006). Moving the arms to activate the legs. *Exercise & Sport Science Reviews, 34*(3), 113–120.
Ford, M. P., Wagenaar, R. C., & Newell, K. M. (2007). Phase manipulation and walking in stroke. *Journal of Neurologic Physical Therapy, 31*, 85–91.
Ford, M. P., Wagenaar, R. C., & Newell, K. M. (2007). The effects of auditory rhythms and instruction on walking patterns in individuals post stroke. *Gait & Posture, 26*(1), 150–155.
Fougner, A., Stavdahl, Ø., Kyberd, P. J., Losier, Y. G., & Parker, P. A. (2012). Control of upper limb prostheses: Terminology and proportional myoelectric control—A review. *IEEE Transactions on Neural Systems and Rehabilitation Engineering, 20*(5), 663–677.
Gil-Agudo, A., Pérez-Nombela, S., Forner-Cordero, A., Pérez-Rizo, E., Crespo-Ruiz, B., & del Ama-Espinosa, A. (2011). Gait kinematic analysis in patients with a mild form of central cord syndrome. *Journal of NeuroEngineering and Rehabilitation, 8*(1), 1–10.
Goudriaan, M., Jonkers, I., van Dieen, J. H., & Bruijn, S. M. (2014). Arm awing in human walking: What is their drive? *Gait & Posture, 40*, 321–326.
Hinrichs, R. N. (1990). Whole body movement: Coordination of arms and legs in walking and running. In J. Winter & S. Woo (Eds.), *Multiple muscle systems* (pp. 694–705). New York: Springer. Ch. 45.
Huang, X., Mahoney, J. M., Lewis, M. M., Guangwei, D., Piazza, S. J., & Cusumano, J. P. (2011). Both coordination and symmetry of arm swing are reduced in Parkinson's disease. *Gait & Posture, 35*(3), 373–377.
Jackson, K., Joseph, J., & Wyard, S. (1978). A mathematical model of arm swing during human locomotion. *Journal of Biomechanics, 11*(6), 277–289.
Kawamura, K., Tokuhiro, A., & Takechi, H. (1991). Gait analysis of slope walking: A study on step length, stride width, time factors and deviation in the center of pressure. *Acta Medica Okayama, 45*(3), 179–184.
Kubo, M., Wagenaar, R. C., Saltzman, E., & Holt, K. G. (2004). Biomechanical mechanism for transitions in phase and frequency of arm and leg swing during walking. *Biological Cybernetics, 91*(2), 91–98.
Kuhtz-Buschbeck, J. P., & Jing, B. (2012). Activity of upper limb muscles during human walking. *Journal of Electromyography and Kinesiology, 22*, 199–206.
Lenhoff, M. W., Santner, T. J., Otis, J. C., Peterson, M. G. E., Williams, B. J., & Backus, S. I. (1999). Bootstrap prediction and confidence bands: A superior statistical method for analysis of gait data. *Gait & Posture, 9*, 10–17.
Major, M. J., Twiste, M., Kenney, L. P. J., & Howard, D. (2014). The effects of prosthetic ankle stiffness on ankle and knee kinematics, prosthetic limb loading, and net metabolic cost of trans-tibial amputee gait. *Clinical Biomechanics, 29*(1), 98–104.
Marigold, D. S., & Misiaszek, J. E. (2009). Whole body responses: Neural control and implications for rehabilitation and fall prevention. *The Neuroscientist, 15*(1), 36–46.
Meyns, P., van Gestel, L., Brujin, S. M., Desloovere, K., Swinnen, S. P., & Duysens, J. (2012). Is interlimb coordination during walking preserved in children with cerebral palsy? *Research in Developmental Disabilities, 33*, 1418–1428.
Nakakubo, S., Doi, T., Sawa, R., Misu, S., Tsutsumimoto, K., & Ono, R. (2014). Does arm swing emphasized deliberately increase the trunk stability during walking in the elderly adults? *Gait & Posture, 40*, 516–520.
O'Brien, R. M. (2007). A caution regarding rules of thumb for variance inflation factors. *Quality & Quantity, 41*(5), 673–690.
Park, J. (2008). Synthesis of natural arm swing motion in human bipedal walking. *Journal of Biomechanics, 41*, 1417–1426.
Park, E. C., & Hwangbo, G. (2015). The effects of action observation gait training on the static balance and walking ability of stroke patients. *Journal of Physical Therapy Science, 27*, 341–344.
Petuskey, K., Bagley, A., Abdala, E., James, M. A., & Rab, G. (2007). Upper extremity kinematics during functional activities: Three-dimensional studies in a normal pediatric population. *Gait & Posture, 25*(4), 573–579.
Pieter, M., Brujin, S. M., & Duysens, J. (2013). The how and why of arm swing during human walking. *Gait & Posture, 38*(4), 552–562.
Pontzer, H., Holloway, J. H., Raichlen, D. A., & Lieberman, D. E. (2009). Control and function of arm swing in human walking and running. *Journal of Experimental Biology, 212*, 523–534.
Prentice, S. D., Hasler, E. N., Groves, J. J., & Frank, J. S. (2004). Locomotor adaptations for changes in the slope of the walking surface. *Gait & Posture, 20*(3), 255–265.

Punt, M., Bruijn, S. M., Wittink, H., & van Dieën, J. H. (2015). Effect of arm swing strategy on local dynamic stability of human gait. *Gait & Posture, 41*, 504–509.
Rab, G., Petuskey, K., & Bagley, A. (2002). A method for determination of upper extremity kinematics. *Gait & Posture, 15*(2), 113–119.
Snee, R. D. (1973). Some aspects of nonorthogonal data analysis, Part I. Developing prediction equations. *Journal of Quality Technology, 5*(1), 67–79.
Stephenson, J. L., Lamontagne, A., & De Serres, S. J. (2009). The coordination of upper and lower limb movements during gait in healthy and stroke individuals. *Gait & Posture, 29*(1), 11–16.
Sylos-Labini, F., Ivanenko, Y. P., MacLellan, M. J., Cappellini, G., Poppele, R. E., & Lacquanti, F. (2014). Locomotor-like leg movements evoked by rhythmic arm movements in humans. *PLoS One, 9*(3).
Tester, N. J., Barbeau, H., Howand, D. R., Cantrell, A., & Behrman, A. L. (2012). Arm and leg coordination during treadmill walking in individuals with motor incomplete spinal cord injury: A preliminary study. *Gait & Posture, 36*, 49–55.
Tester, N. J., Howland, D. R., Day, K. V., Suter, S. P., Cantrell, A., & Behrman, A. L. (2011). Device use, locomotor training and the presence of arm swing during treadmill walking after spinal cord injury. *Spinal Cord, 11*(49), 451–456.
Tulchin, K., Orendurff, M., & Karol, L. (2010). The effects of surface slope on multi-segment foot kinematics in healthy adults. *Gait & Posture, 32*(4), 446–450.
Wagenaar, R. C., & van Emmerik, R. E. (1994). Dynamics of pathological gait. *Human Movement Science, 13*, 441–471.
Wagenaar, R. C., & van Emmerik, R. E. (2000). Resonant frequencies of arms and legs identify different walking patterns. *Journal of Biomechanics, 33*(7), 853–861.
Webb, D., Tuttle, R., & Baksh, M. (1994). Pendular activity of human upper limbs during slow and normal walking. *American Journal of Physical Anthropology, 93*, 477–489.
Winter, D. A. (2005). *Biomechanics and motor control of human movement* : . John Wiley & Sons, Inc.
Wu, Y., Li, Y., Liu, A.-M., Xiao, F., Wang, Y.-Z., Hu, F., ... Gu, D.-Y. (2016). Effect of active arm swing to local dynamic stability during walking. *Human Movement Science, 45*, 102–109.
Yoon, J., Novandy, B., Yoon, C. H., & Park, K. J. (2010). A 6-DOF gait rehabilitation robot with upper and lower limb connections that allows walking velocity updates on various terrains. *IEEE Transactions on Mechatronics, 15*, 201–215.